International Journal of Chemistry; Vol. 6, No. 1; 2014
ISSN 1916-9698 E-ISSN 1916-9701
Published by Canadian Center of Science and Education

Application of Pt.TiO_2 Nanofibers in Photosensitized Degradation of Rhodamine B

Emilly A. Obuya[1], Prakash C. Joshi[1], Thomas A. Gray[1], Thomas C. Keane[1] & Wayne E. Jones Jr.[2]

[1] ISES Labs, Department of Chemistry and Biochemistry, Russell Sage College, Troy, NY, USA

[2] Department of Chemistry, State University of New York at Binghamton, Vestal, NY, USA

Correspondence: Thomas C. Keane, Director, ISES Labs, Department of Chemistry and Biochemistry, Russell Sage College, Troy, NY 12180, USA. Tel: 1-518-244-2299. E-mail: keanet@sage.edu

Received: September 11, 2013 Accepted: October 8, 2013 Online Published: November 21, 2013

doi:10.5539/ijc.v6n1p1 URL: http://dx.doi.org/10.5539/ijc.v6n1p1

Abstract

The surface properties of TiO_2 nanofibers were utilized for the *in-situ* and *ex-situ* nucleation and growth of metal nanoparticles. Pt nanoparticles were generated on the titania surface without the use of external stabilizing agents. These nanoparticles were effectively anchored on the numerous pores present on the TiO_2 surface and acted as sites for continued nanoparticle growth. The TiO_2 surface exhibited extensive folding resulting in increased surface area that was then explored for the effective adsorption of reacting materials for heterogeneous catalysis. The resulting TiO_2-based catalysts were found to facilitate UV/Visible light sensitized degradation of Rhodamine B (RH-B). The photodegradation followed first order kinetics with a rate constant of 0.0158 min^{-1}. An investigation of the mechanism of RH-B degradation suggests a role of reactive oxygen species (ROS) as intermediates in the photodegradation process.

Keywords: electrospinning, transition metal nanoparticles, polyol technique, photodegradation, electron-hole recombination, rhodamine B

1. Introduction

Heterogeneous photocatalysis is an emerging area of research (Mills & Hunte, 1997; Bouras et al., 2007). The most commonly used photocatalyst has been titanium dioxide, which is a wide-band gap (~3.0-3.2 eV) semi-conductor metal oxide. The photocatalytic activity of a semi-conductor is due to the photo-induced electron-hole pairs created by illumination with light. These energetically excited species can be harvested to generate electricity in solar cells or in chemical processes for the degradation of organic pollutants (Carp et al., 2004; Guo et al., 2011). Titania-based materials have gained much interest in environmental remediation due to their transparency to visible light, high refractive index, low absorption coefficient, chemical stability, non-toxicity and cost effectiveness (Kwon et al., 2004; Wang et al., 2008). Some of the commercial applications of titania include antibacterial action and waste water treatment (Kwon et al., 2004; Im et al., 2009). Due to its wide band gap, UV light is required to generate electron-hole pairs. This significantly limits titania as an effective photocatalyst since UV light accounts for only 5% of total solar radiation. Additionally, the fast recombination rate of photogenerated electron-hole pairs lowers the photocatalytic efficiency (Zhu et al., 2008). To solve these problems, numerous research efforts are currently focused on the generation of novel materials that will shift the optical response of the photocatalyst to the visible range while preventing the recombination of the photogenerated electrons and hole (Friedmann et al., 2010; Fu et al., 2011; Sakthivel et al., 2006)

A popular approach used to shift the optical absorption of titania from UV to visible range has been doping with transition metal elements (Wang et al., 2008; Zhu et al., 2008; Seery et al., 2007) non-metal ions (Im et al., 2009; Guo et al., 2010), dye-sensitization (Kozuka et al., 1996) and semi-conductor coupling (Liu et al., 2009; Wang et al., 2004). The role of the transition metal/non-metal doping is to introduce trapping sites that would scavenge the photogenerated electrons to separate the electron-hole pairs (Yalda et al., 2010; Ali et al., 2011), thus promoting redox processes on the catalyst surface (Bouras et al., 2007; Wang et al., 2008; Zhu et al., 2008). Further, dopants shift the absorption maximum of titania to the visible range by introducing energy states within the semi-conductor band gap that lower the energy required for excitation and hence the use of direct solar radiation (Bouras et al., 2007). The doped titania materials have been actively used in photosensitization reactions as useful means of detoxification of environmental pollutants (Wang et al., 2009; Kment et al., 2010).

Photosensitization reactions are also involved in effective therapies for the control of certain types of cancer, psoriasis, vitiligo and other skin diseases (Smith, 1989). Photosensitization technology has previously been employed for the purification of contaminated water, infectious blood and controlling neonatal bilirubemia (MacCormack, 2008; Pasale et al., 1976; Pillay & Salih, 2004).

The traditional methods used for the environmental remediation of organic pollutants have not been very effective, since they only transform the organic molecules from one form to another without complete degradation (Chumcheng et al., 2010). Furthermore, the mechanism for degradation of these dyes remains unclear. It is well established that reduction of particle size has a marked influence on increasing the system's catalytic activity. The shift to nanostructured materials for photocatalysis is a very active area of research in order to obtain materials with high surface areas and large pore volumes for enhanced dispersion and catalytic activity (Zhang et al., 2008; Libanori et al., 2009). The aspect ratios for nanostructured materials shortens the transportation length of electrons and holes from the crystal interface to the surface, thus accelerating their migration to the surface for redox reactions (Wang et al., 2008).

This paper highlights the synthesis and characterization of a new type of nanostructured TiO_2-based material with efficient electron-hole charge separation and high specific surface areas. We have explored the electronic and surface structures of titania nanofibers for the deposition of Pt nanoparticles via comparison of a modified *in-situ* with a newly developed *ex-situ* polyol synthesis procedure. Rhodamine B, a triphenylmethane dye (Yu et al., 2009; He et al., 2009a, 2009b) was used to probe catalytic activity. Visible light was harvested by the doped TiO_2 for a more efficient and sustainable process while the nanoparticles acted as effective electron traps to prevent recombination of the TiO_2 electron-hole pair. An investigation of the involvement of ROS in Pt-TiO_2 sensitized degradation of the dye under UVA was undertaken to facilitate an understanding of as plausible mechanistic pathway of the reactive species on the TiO_2 surface.

2. Experimental

2.1 Materials

Catalase, deoxyguanosine (dGuo), ethylene glycol (EG), histidine, hydrogen peroxide (H_2O_2), mannitol, N,N-dimethylformamide (DMF), N,N-dimethyl-p-nitrosoaniline (RNO), chloroplatinic acid hydrate ($H_2PtCl_6.xH_2O$), polymethymethacrylate (PMMA), polyvinyl pyrrolidone (PVP), Rhodamine B (RH-B), riboflavin (RF), rose bengal (RB), sodium azide (NaN_3), sodium bicarbonate ($NaHCO_3$), sodium carbonate (Na_2CO_3), sodium phosphate dibasic (Na_2HPO_4), sodium phosphate monobasic (NaH_2PO_4), superoxide dismutase (SOD) and titanium isopropoxide (TiP) were purchased from Sigma/Aldrich Chemical Company, St. Louis, MO, and were used as received.

2.2 Instrumentation

The PMMA/TiP nanofibers were electrospun using a high KV Spellman SL 30 generator. The morphology and size of the fibers were determined using a Hitachi S-570 or Supra Zeiss 55VP Scanning Electron Microscope (SEM), equipped with an EDAX system for Energy Dispersive Spectroscopic (EDS) analysis. Transmission Electron Microscopy (TEM) images of the catalysts was obtained on a JEOL 2010 FETEM instrument. The samples were dispersed in ethanol by sonication. The resulting solution was placed onto a lacey carbon-coated Cu grid. UV-Visible determinations were done on an 8452A Hewlett Packard Diode Array spectrophotometer instrument in the 190 to 820 nm range. The ultraviolet irradiation system comprised a horizontal planar array of three, 4-foot long UVA-emitting (320–400 nm, TL-D 36 W), fluorescent tubes manufactured by Philips, Holland. The irradiance of the emitted light was measured by a VLX-3W UVR probe which was equipped with UVA (SX-365nm), UVB (290–320 nm, SX-312nm) and UVC (180–290 nm, SX-254nm) detectors, manufactured by Vilber Lourmat, Marne La Valle, France. The UVR dose is expressed in Joules (J = W/cm^2 x Second). The irradiance output of UVA was 5.8 mW/cm^2 at a distance of 10 cm from the source. The interference of UVB in the UVA source was below 0.2 mW/cm^2. No UVC was detected in the UVA source.

3. Methods

3.1 Fabrication of TiO_2 Nanofibers

The detailed procedure has been described earlier (Obuya et al., 2011). Briefly, a solution of TiP was mixed with PMMA to achieve a viscous polymer blend. For the electrospinning process, a high voltage power supply (25 kV/cm) induced electrical charges on the polymer blend to stretch the solution into submicron length fibers. DMF was added to ensure a dielectric constant sufficient to withstand the high electric voltages. As the solvents evaporated, the stretched PMMA/TiP fibers were collected on an aluminum foil attached to the collector plate. TiO_2 nanofibers were then synthesized after heat treatment at 500 ^oC to remove the polymer matrix.

3.2 Deposition of Pt Nanoparticles on the Surface of the TiO_2 Nanofibers

3.2.1 *In-Situ* Polyol Deposition

EG (10 ml) was heated at 110 ^oC in an oil bath (30 minutes) followed by addition of TiO_2 fibers. The EG/TiO_2 mixture was irradiated under UV light for 30 minutes. Subsequently, Pt^{2+} and PVP (1:20 mole ratio) were added to the EG solution, which was left stirring for an additional 30 minutes to control the nucleation process of the nanoparticles. At the end of the reaction, the catalyst was washed several times with acetone, centrifuged and dried in an oven at 120 ^oC for 3 h to remove residual PVP and EG.

3.2.2 *Ex-Situ* Polyol Deposition

EG (10 mL) was heated in an oil bath at 110 ^oC (60 minutes), followed by addition of a 1:5 mole ratio of Pt^{2+}: PVP to initiate the nucleation process. This solution was left stirring for 60 minutes, after which it was immediately cooled in ice to stop further growth of the Pt nanoparticles. The Pt nanoparticles (in 2 mL ethanol) were dispersed on the surface of the TiO_2 nanofibers with sonication (120 minutes). The catalysts were cleaned and dried via steps described in section 3.2.1.

3.3 A Probe of the Catalyst Efficiency

3.3.1 Photodegradation of RH-B

Pt-TiO_2 catalyst (50 mg) was sonicated in 10 mL distilled water (15 minutes) to ensure complete dispersion of nanoparticles in solution. The catalyst was mixed with a 10^{-5} M solution of RH-B in distilled water (50 mL) for 30 minutes in the dark to reach an adsorption/desorption equilibrium. The mixture was continuously stirred in air and irradiated under UV light. The distance between the UV lamp and the reaction beaker was maintained at 20 cm. The progress of reaction was monitored by recording the absorption spectra of irradiated samples after every 10 minutes. Aliquots (0.5 ml in 5 mL H_2O) were centrifuged at 1550 RPM for 30 minutes to remove the dispersed catalyst before recording the absorption spectrum. Control experiments included: (i) dye with UV light in the absence of catalyst, (ii) both *in-situ* and *ex-situ* Pt-TiO_2 in sunlight, (iii) undoped TiO_2 nanofibers under UV light and (iv) undoped TiO_2 in sunlight.

3.3.2 Mechanism of Photodegradation

RH-B degradation with the *in-situ* Pt-TiO_2 was carried out under three different conditions: (i) irradiation in 0.01M phosphate buffer, pH 7.0, (ii) irradiation in the presence of Pt-TiO_2 as a photosensitizer, pH 7 and (iii) irradiation in the presence of Pt-TiO_2 and selected scavengers of free radical/reactive O_2 species (ROS) scavenger. 20 mL samples of a 6.25×10^{-6} M solution of RH-B (prepared in pH 7 phosphate buffer) were irradiated in a Petri dish with or without a sensitizer (10.0 μg/mL) or varying amounts of a quencher under UVA at a dose ranging from 2 to 20 J.

4. Results and Discussion

4.1 Scanning Electron Microscopy and Energy Dispersive Spectroscopy

SEM analysis of the TiO_2 nanofibers indicated an enlarged surface area that was highly folded and wrinkled, providing favorable sites for heterogeneous nucleation of metal nanoparticles (Figure 1). In Figure 2, a highly magnified SEM image shows the presence of numerous pores that are indicative of a mesoporous structure of the TiO_2 that allows for the effective absorption of reacting molecules. This porosity, coupled with its ability to create photoinduced electron-hole pairs makes it a very effective support for the *in-situ* synthesis of nanoparticles without the need for external stabilizing agent. Figure 3 illustrates EDS image that shows the elemental composition and distribution of the *in-situ* Pt-TiO_2 catalysts, where the presence of a carbon peak on both spectra is indicative of incomplete combustion of PMMA.

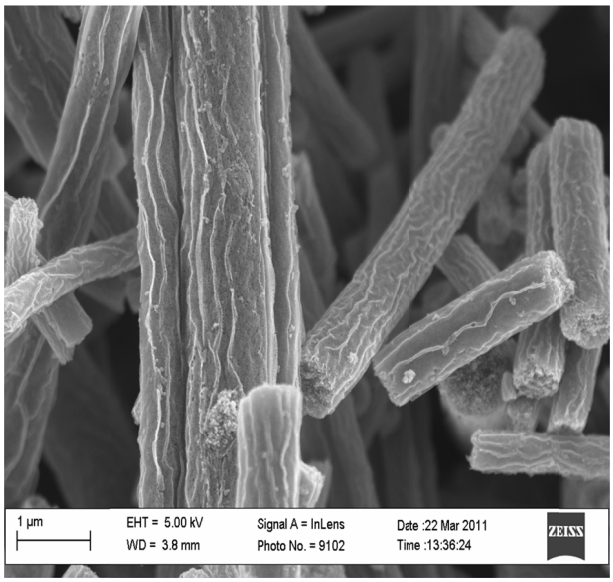

Figure 1. SEM image of doped TiO_2 catalyst showing folding of the titania nanofibers that provides a high surface area and stabilization of the metal nanoparticles

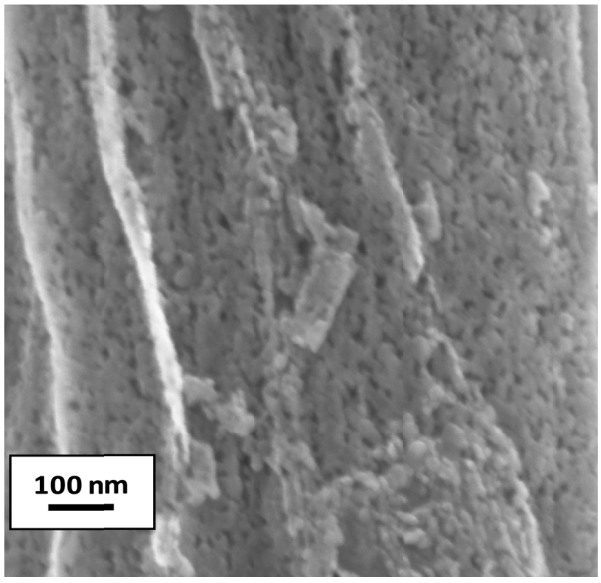

Figure 2. SEM image of TiO_2 nanofibers showing the porous nature of the titania surface

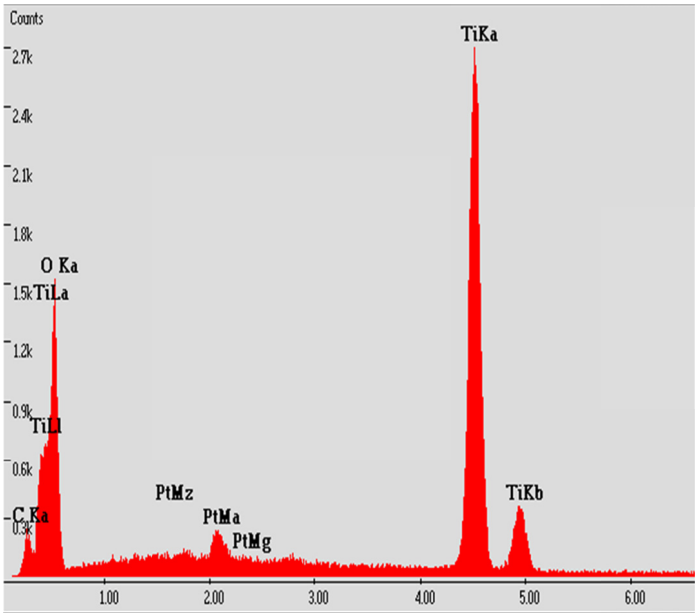

Figure 3. EDS spectrum of 5 wt. % Pt-TiO_2 produced by the *in-situ* method, showing presence of Pt, Ti and O and their relative distributions

4.2 Transmission Electron Microscopy

4.2.1 Particle Size

The surface interstitial sites, as well as the porosity of the TiO_2 surface enabled the *in-situ* nucleation, growth and stabilization of Pt nanoparticles of ~4 nm (Figure 4). These nanoparticles remained stabilized over an extended period of time hence their viability as heterogeneous photocatalysts for RH-B degradation. For *ex-situ* deposition, Pt nanoparticles of ~3.7 nm were synthesized (Figure 5). These Pt nanoparticles were successfully dispersed on TiO_2 surface without losing their integrity (Figure 6).

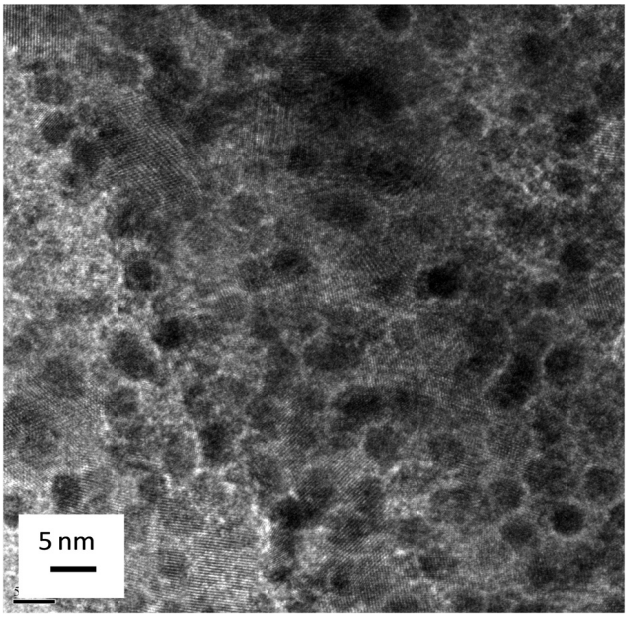

Figure 4. TEM image showing TiO_2 nanofiber surface decorated with ~4 nm Pt nanoparticles deposited via the *in-situ* method

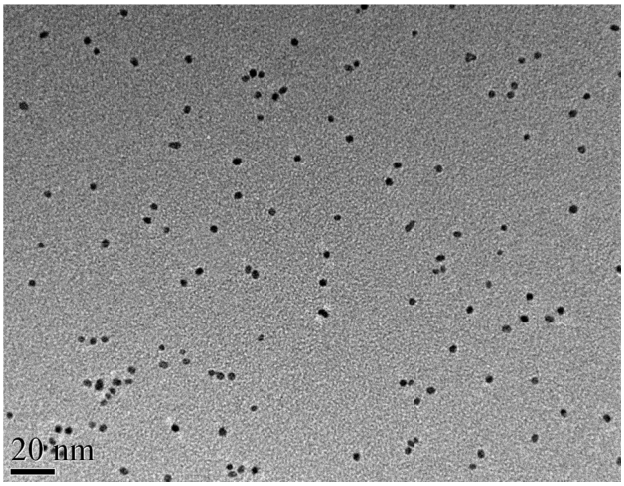

Figure 5. TEM image of Pt nanoparticles of ~3.7 nm deposited via the ex-situ method

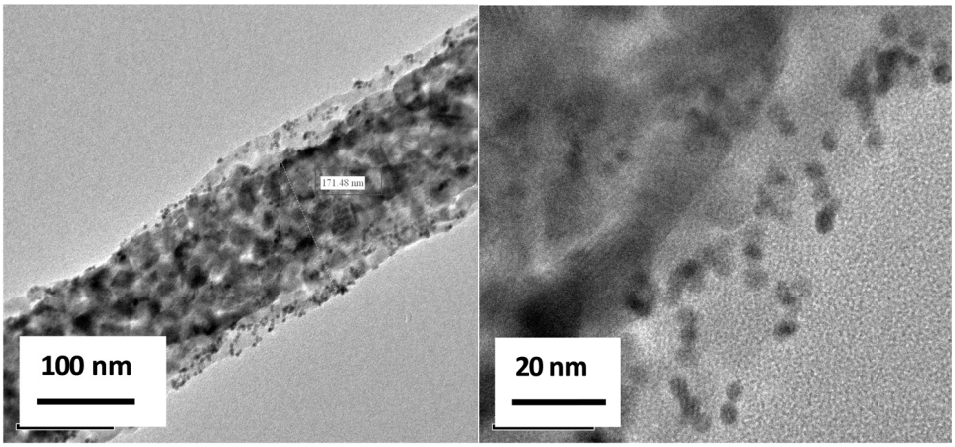

Figure 6. TEM image of ex-situ Pt nanoparticles after dispersion on the TiO_2 surface. The Pt nanoparticles maintained their integrity without agglomeration

4.2.2 Energy Dispersive Spectroscopy for an Isolated Spot on a TEM Image

Elemental analyses for isolated dark spots on the TEM images were carried out to ascertain that these were nanoparticles. For *ex situ* deposited Pt-TiO_2, the EDS spectra showed a strong Pt peak, indicating the significant presence of Pt nanoparticles (Figure 7).

4.2.3 Powder X-Ray Diffraction (PXRD) Analysis

PXRD patterns for the Pt-TiO_2 and bare TiO_2 nanofibers suggest that the crystalline structures for the catalysts are predominantly anatase phase with a very small rutile percentage for the TiO_2 nanofibers (Figure 8). The pattern for the Pt-TiO_2 catalyst shows extra peaks (at 2 theta values of 40 and 47) which are indicative of the presence of Pt nanoparticles.

XPS analysis was done in order to study the nature of surface interactions for the TiO_2 based catalysts (Figure 9). This study was performed with three catalysts prepared under the following conditions; (i) TiO_2 nanofibers calcined under air at 600 ^oC with a 1h hold time (TiO_2_air); (ii) TiO_2_H_2 with similar preparation conditions as TiO_2_air but with calcination under hydrogen gas and (iii) Pt-TiO_2 where the TiO_2_air catalyst underwent an additional polyol deposition of Pt nanoparticles (this procedure is briefly outlined in the experimental section).

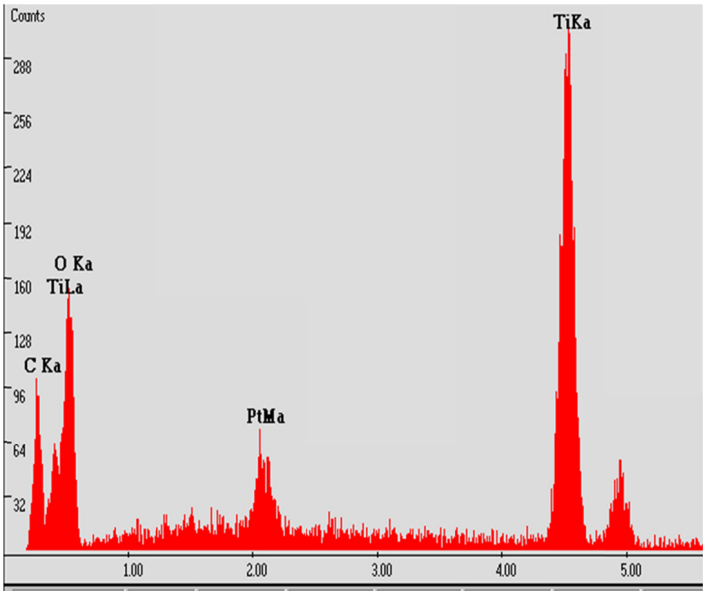

Figure 7. EDS spectrum of Pt-TiO_2 produced by the ex-situ method, showing presence of Pt, Ti and O and their relative distributions

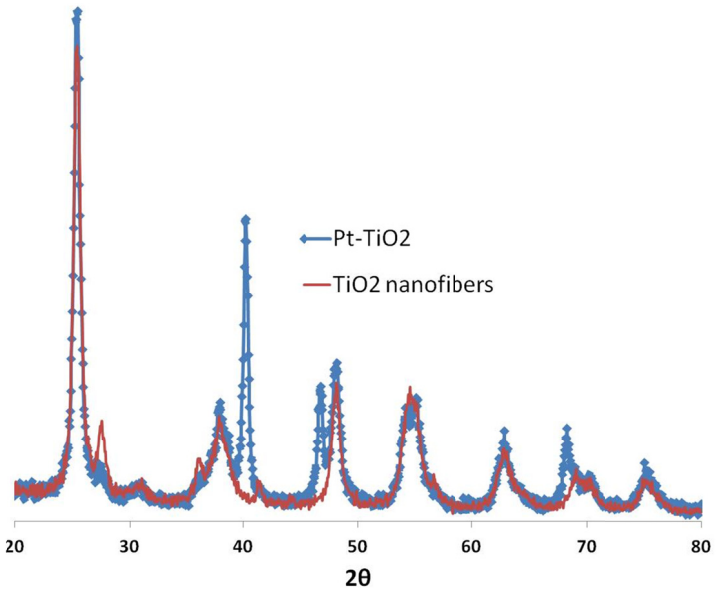

Figure 8. PXRD patern for Pt-TiO_2 and TiO_2 nanofibers showing new peaks (between 2 theta values of 40 and 50) that correspond to Pt nanoparticles

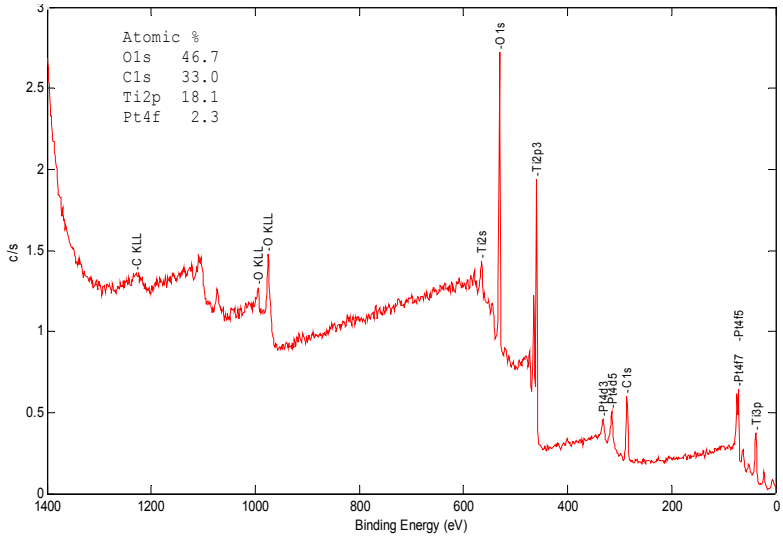

Figure 9. XPS spectra showing atomic percentages of the elements present in Pt-TiO_2 catalyst

Table 1. A summary of the elemental composition and atomic percentage of the Pt-TiO_2 catalyst

Pt-TiO_2		O/Ti ratio is 39.5/18.4 = **2.15**			ΔB.E of O - Ti = 529.7 - 458.5= **71.2**			
Atomic % from XPS spectrum		**Peak**	**B.E (eV)**	**Peak assignment**	**Area**	**Area ratio**	**Area %**	**FWHM**
Pt	2	4f5/2	70.6	Pt	N/A	N/A	N/A	N/A
Ti	18.4	2p3/2	**458.5**	Ti in TiO_2	7900	N/A	N/A	1.03
C	32.2	1s	284.8	C-C, C-H	1915	0.67	21.4	1.65
			286.3	C-OH,C-O-C	368	0.13	4.12	1.72
			283.6	CO/Pt/Ti	324	0.11	3.63	1.24
			288.4	O--C=O	267	0.09	2.99	1.64
O	47.3	1s	**529.7**	O in TiO_2	8838	0.84	**39.5**	1.20
			531.4	Adsorbed O	1737	0.16	7.76	1.62

A summary of the elemental composition and relative percentages of the Pt-TiO_2 catalysts obtained from the XPS spectrum is given in Table 1. It provides the atomic percentages, binding energies, and peak areas for each assigned peak for Ti, O, C and Pt elements. These binding energies are used for peak identification against known values so as to establish the electronic states of the elements, while the atomic percentages and peak areas are used to calculate the percentage of O bonded to Ti, C and/or adsorbed on the TiO_2 surface. The Pt 4f5/2 peaks that were observed at binding energies of 70.6 and 74.0 eV were assigned to elemental Pt.

4.2.4 Catalytic Activity of Titania Nonofibers

The semiconductor nature of titania nanofibers was explored for the *in-situ* reduction of metal ion precursors on the TiO_2 surface using conduction band electrons. The presence of oxidizable additives, in our case EG, made use of the valence band holes thereby preventing electron-hole recombination. The *ex-situ* method was preferred for the Pt-TiO_2 catalyst since more of the nanoparticles were available on the TiO_2 fiber surface, which resulted in improved adsorption and degradation of organic pollutants. The objective of loading TiO_2 with nanoparticles was to maximize the extension of the existing wavelength response of the catalyst to longer wavelength (visible) region. The Pt nanoparticles also provided enhanced charge mobility on the TiO_2 surface thus preventing electron-hole recombination.

4.2.5 Photodegradation of RH-B

Photodegradation of RH-B was recorded by monitoring the disappearance of absorption of RH-B at ~554 nm with time (Figure 10). The control experiment, which was carried out under the same conditions, on the same day but without the catalyst, shows no significant disappearance of the RH-B peak (Figure 11). Figure 12 shows that in reactions carried out without catalyst, the dye was not degraded even after 240 minutes, while the highest activity was recorded with Pt-TiO_2 under sunlight.

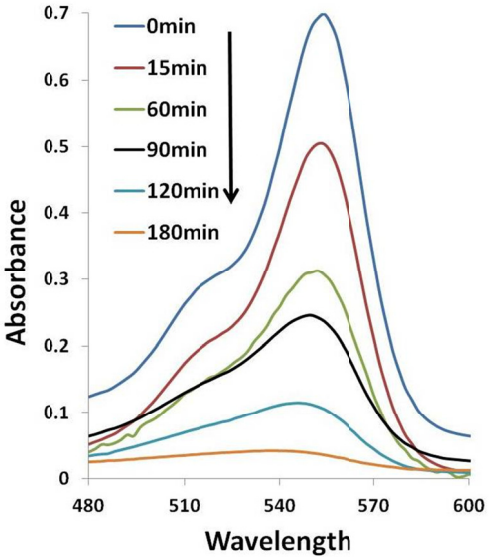

Figure 10. Photodegradation of RH-B with in-situ Pt-TiO_2 in sunlight

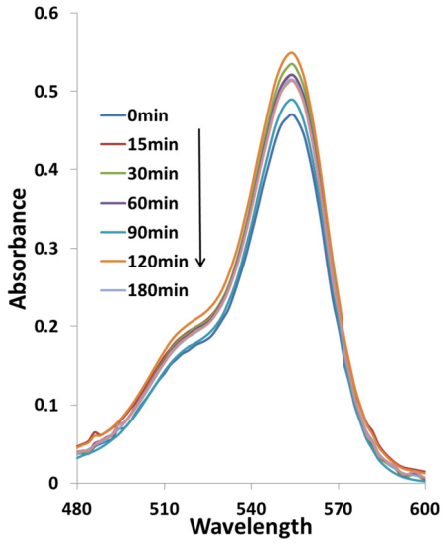

Figure 11. Control experiment for photodegradation of RH-B in sunlight (without the Pt-TiO_2 catalyst)

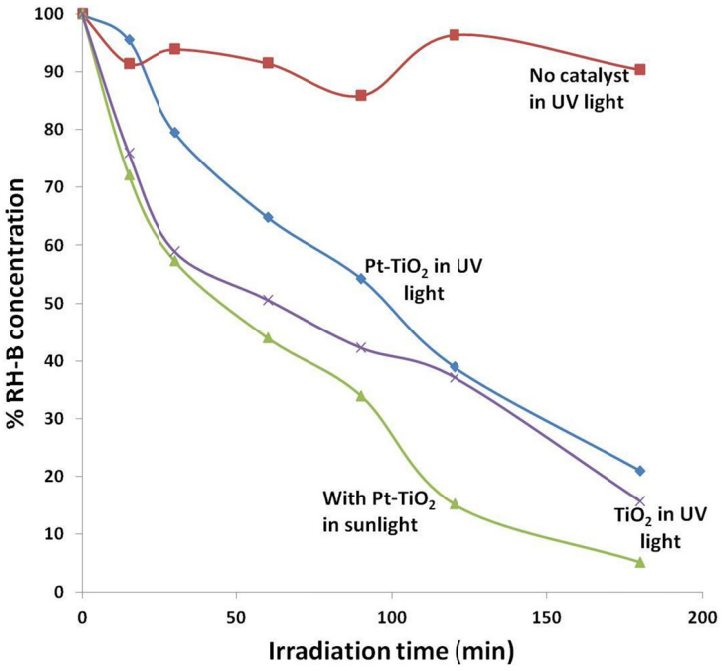

Figure 12. Comparison of RH-B degradation with different catalysts

4.3 Investigation of the Involvement Reactive Oxygen Species (ROS) in the Photodegradation of RH-B

The photosensitization mechanism is classified into two different categories based on their requirement of O_2: (1) Type I, O_2-independent reactions, where the sensitizer is often consumed in the reaction (Pathak & Joshi, 1983) and (2) Type II, O_2-dependent reactions termed as photodynamic action (Foote, 1991). In photodynamic reactions, it is recognized that singlet oxygen ($^1O_2$), superoxide anion radicals ($O_2^{-}\cdot$), hydroxyl radicals ($^{\cdot}OH$) and hydrogen peroxide (H_2O_2) are formed. Interconversion of these reactive species is also possible as shown schematically in Figure 13 (Pathak & Joshi, 1983).

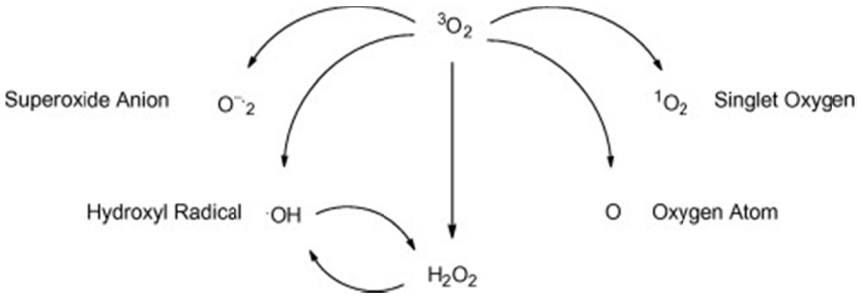

Figure 13. Interconversion of reactive oxygen species

4.3.1 Investigation of the Involvement of Singlet Oxygen ($^1O_2$) in Photodegradation

Involvement of $^1O_2$ in the photosensitized degradation of RH-B was determined by carrying out Pt-TiO_2 sensitized photodegradation of RH-B in the presence of sodium azide (NaN_3) which is a well-recognized scavenger of $^1O_2$ (Das & Misra, 2004). NaN_3 was used at two different concentrations (10 mM and 2.5 mM). The photodegradation of RH-B was not affected by the presence of NaN_3 at any of these conditions indicating that $^1O_2$ was not involved in its photodegradation. Another method for an indirect determination of $^1O_2$ was used by studying photosensitized degradation of a guanine analog of DNA/RNA (Joshi, 1998).

As shown in Table 2, Pt-TiO_2 sensitized degradation of dGuo was studied to confirm that $^1O_2$ is not involved in the photodegradation of RH-B. A 0.1 mM solution of deoxyguanosine (dGuo) was prepared in 0.01 M carbonate buffer (pH, 10) and 20 mL aliquot was irradiated in a petri dish under UVA for a dose ranging from 0 to 10 Joule.

The results were compared with well recognized $^1O_2$ generating photosensitizers like RF and RB. While photosensitized RF and RB degraded dGuo by 99.1 ± 0.3% and 50.8 ± 1.6%, respectively, the Pt.TiO_2 photocatalyst was relatively ineffective (3.5 ± 0.1% degradation) under similar conditions. The photodegradation of dGuo by RF and RB was inhibited by over 95% with 10 mM NaN_3 (Joshi, 1985).

Table 2. A comparison of photosensitized degradation of deoxyguanosine by Pt-TiO_2, Riboflavin (RF) and Rose Bengal (RB) under UVA

Reaction Mixture	Concentration of Photosensitizer (µg/mL)	UVADose (Joule)	Photodegradation (%)
dGuo + Buffer	-	10.0	0.00
dGuo + Pt-TiO2	3.50	3.50	0.9 ±0.01
dGuo + Pt-TiO2	7.00	7.00	3.0 ±0.10
dGuo + Pt-TiO2	10.0	10.0	3.5±0.01
dGuo + RF	3.50	3.50	73.0 ±0.4
dGuo + RF	7.00	7.00	94.9 ± 0.1
dGuo + RF	10.0	10.0	99.1 ± 0.3
dGuo + RB	3.50	3.50	27.2 ± 2.4
dGuo + RB	7.00	7.00	44.8 ± 1.9
dGuo + RB	10.0	10.0	50.8 ± 1.6

The results of this study suggest that photosensitized degradation of dGuo by RF and RB is largely due to the involvement of $^1O_2$. However, Photosensitized Pt-TiO_2 did not show significant involvement in dGuo degradation providing additional evidence that its involvement in RH-B photodegradation was not due to $^1O_2$. In order to reconfirm this result, $^1O_2$ determination test were carried out with Pt-TiO_2, RF, RB and RH-B in an experiment described below.

4.3.2 Determination of $^1O_2$ Generation by Pt-TiO_2 and Its Comparison With Riboflavin, Rose Bengal and RH-B

The production of $^1O_2$ by photosensitized Pt-TiO_2, RF, RB and RH-B under aerobic condition was measured in an aqueous solution by literature procedure (Kraljic & El Moshni, 1978). $^1O_2$ forms transannular peroxide intermediate with histidine leading to the bleaching of RNO, which was quantitatively measured spectrophotometric ally at 440 nm. The results confirmed that Pt-TiO_2 and RH-B were not major producers of $^1O_2$ as compared to RF and RB, Figure 14.

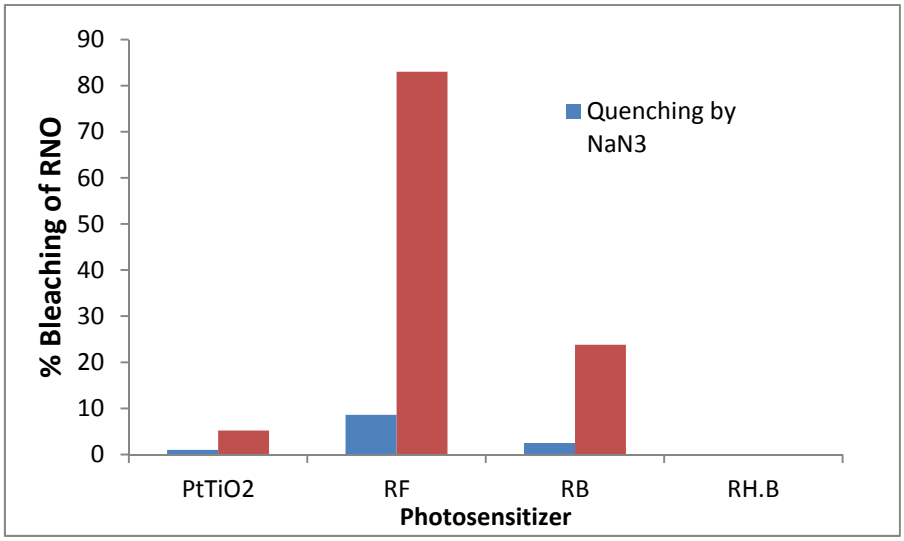

Figure 14. Formation of $^1O_2$ by various test compounds as determined by the bleaching of RNO (red) and quenching by sodium azide (blue)

4.3.2.1 Role of Superoxide Anion Radicals ($O_2^{-}\cdot$) in the Photodegradation of RH-B

The involvement of $O_2^{-}\cdot$ in the Pt-TiO_2 sensitized (UVA, 20J) degradation of RH-B was determined by carrying out the photosensitized reaction in the presence of 25 U/μL SOD (Beauchamp & Fridovich, 1971). The photodegradation was not affected by SOD indicating no involvement of $O_2^{-}\cdot$ in the reaction.

4.3.2.2 Role of Hydroxyl Radicals ($^{\cdot}OH$) in the Photodegradation of RH-B

The involvement of $^{\cdot}OH$ in the Pt-TiO_2 sensitized degradation of RH-B was determined by carrying out the reaction in the presence of mannitol (10 mM; Goldstein & Czapski, 1984). Photodegradation of RH-B was inhibited by 74.4% in the presence of mannitol indicating that $^{\cdot}OH$ was involved in the reaction.

4.3.2.3 Role of Hydrogen Peroxide (H_2O_2) in the Photodegradation of RH-B

The involvement of H_2O_2 in the photosensitized degradation of RH-B was determined by carrying out reaction in the presence of catalase (Seaver & Imlay, 2001). A stock solution of catalase (100 mg/mL) was prepared in phosphate buffer (0.01 M, pH 7) and 400μg/mL aliquot was added to the irradiation solution of RH-B. The Pt-TiO_2 sensitized degradation of RH-B was inhibited by 47.8% in the presence of catalase indicating partial involvement of H_2O_2 in the reaction.

4.4 Mechanism of RH-B Photodegradation

RH-B structure contains four N-ethyl groups on either side of the xanthene ring and a carboxylic acid group on the phenyl group connected to the xanthene ring (Figure 15).

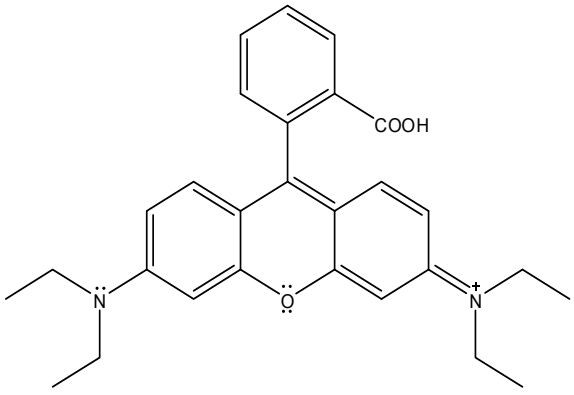

Figure 15. Chemical structure of Rhodamine B

The presence of non-bonded lone pairs of electrons on the functional groups and the extended π conjugation makes this molecule susceptible to attack by ROS produced by oxidative and reductive pathways on the semiconductor surface (Wu et al., 1998). The positively charged amine groups assists in the adsorption of RH-B onto the negatively charged TiO_2 surface. Previous reports suggest that the photocatalytic cleavage of the RH-B molecule takes place via two competitive processes; N-de-ethylation and chromophore cleavage (He et al., 2009b). Subsequently, ring opening and mineralization occurs to give rise to various products.

For this study, UV-Vis absorption data were used to track the degradation process; chromophore cleavage of the dye led to the destruction of π conjugation across the RH-B molecule and thus the complete disappearance of the absorption maximum band at 554 nm (Figure 10). Due to its auxochromic properties, the stepwise removal of the N-ethyl group lead to a consistent hypsochromic shift of the absorption maximum band at 554 nm. A consistent decrease in the absorption at 554 nm with a simultaneous increase in absorption at ~248 nm (Figure 16) suggested the degradation of RH-B with the formation of lower wavelength-absorbing photoproducts. The identification of photoproducts is the subject of our ongoing research. Chromophore cleavage of RH-B under microwave irradiation using graphite-supported TiO_2 or Bi_2WO_6 as catalysts proceeds through the formation of benzoic, hydroxybenzoic, phthalic and terephthalic acids, as identified by GC/MS analysis (He et al., 2009a, 2009b; Wu et al., 1998). Based on the experiments showing the participation of $^{\cdot}OH$ and H_2O_2 in RH-B degradation, a mechanism for RH-B degradation involving ·OH has been proposed (Figure 17). The N-de-ethylation is initiated by the attack on an ethyl group of the RH-B molecule by $^{\cdot}OH$. The resulting radical undergoes β-cleavage to generate a stabilized radical and ethylene, which abstracts a hydrogen atom from water

to regenerate the hydroxyl radical. This chain reaction can proceed until all the ethyl groups are removed from the molecule.

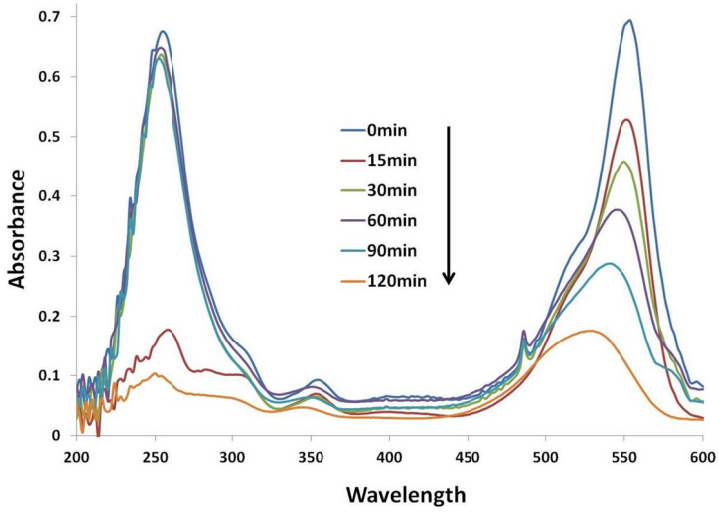

Figure 16. UV-Vis analysis showing the degradation of RH-B by the decrease in absorption at 554 nm and formation of new photoproducts shown by an increase in the absorbance at 248 nm

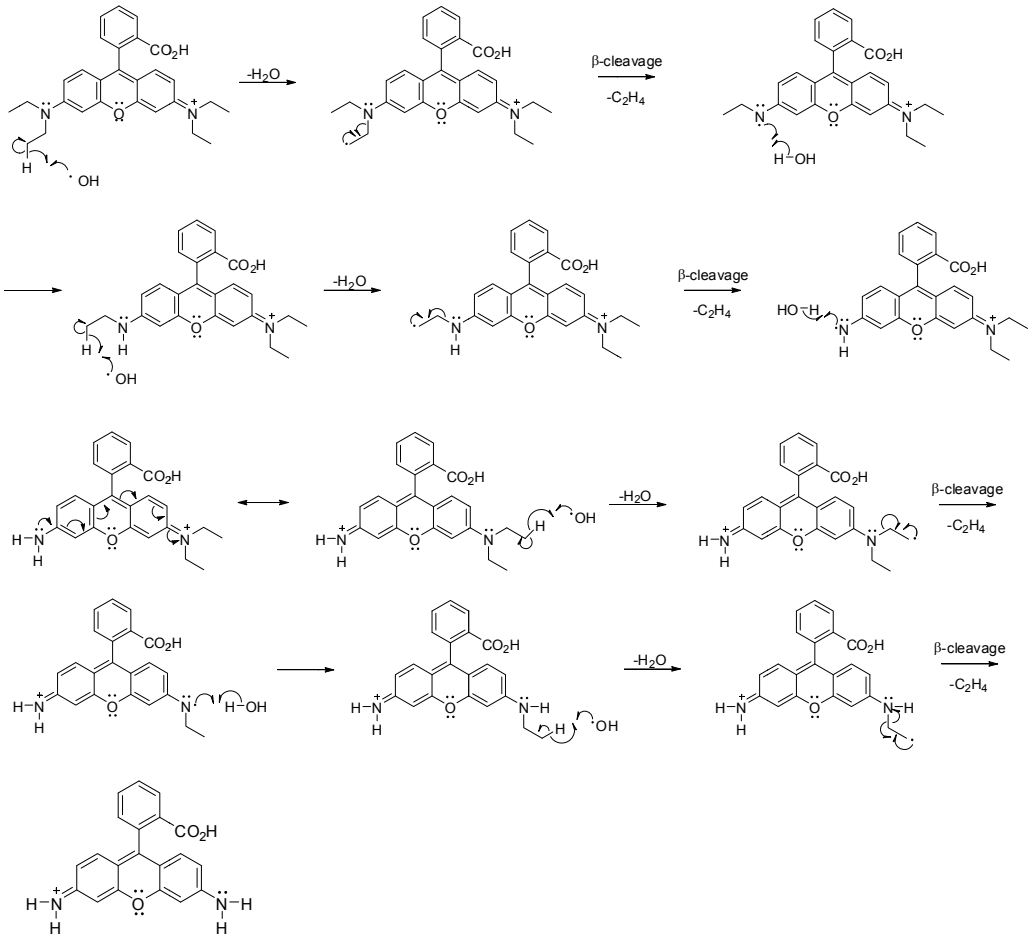

Figure 17. The proposed mechanism for N-de-ethylation of RH-B on the TiO_2 surface

5. Conclusion

An efficient Pt-TiO_2 catalyst was prepared by a modified *ex-situ* polyol method. The mesoporous nature of the TiO_2 nanofibers, coupled with a large surface to volume ratio provided a suitable anchorage for the Pt nanoparticles. Additionally, the TiO_2 surface was crucial for the adsorption of RH-B and the generation of ROS required for the degradation reaction. Maximum degradation using Pt-TiO_2 was observed in sunlight, which followed a first order reaction kinetics, with a rate constant of 0.0158 min^{-1}. Presence of Pt nanoparticles provided additional active sites for the adsorption of reactive intermediates as well as improved charge mobility on the TiO_2 surface, thereby preventing electron-hole recombination. Quenching studies suggested that $^{\cdot}OH$ and H_2O_2 were responsible for the Photodegradation of RH-B, while $^1O_2$ and $O_2^{-\cdot}$ were not involved. These observations were in agreement with earlier studies on photosensitization reactions of Pt-TiO_2 complexes where damage to protein and DNA analogues was demonstrated via formation of $^{\cdot}OH$ and H_2O_2 (Macyk & Kisch, 2001; Hirakawa et al., 2004). This study provided useful information on the role of selective ROS as intermediates in the photocatalytic degradation of RH-B.

Acknowledgements

The authors wish to acknowledge Timothy O'Brien, an undergraduate student at SUNY, Binghamton who contributed to catalyst fabrication and Rhodamine B degradation experiments. Hsin Li, Monique Merchant and Erica Dobroski, undergraduate students at Russell Sage College (RSC) contributed to discussions of the proposed mechanism for Rhodamine B degradation. We are especially indebted to Donna Robinson Esteves (RSC '70) for providing financial support for the Laboratories for Interdisciplinary Studies in Emerging Sciences (ISES), the academic research arm of the Incubator for New Ventures in Emerging Sciences and Technologies (INVEST) at Russell Sage College.

References

Ali, A. M., Emanuelsson, E. A. C., & Patterson, D. A. (2011). Conventional versus lattice photocatalysed reactions: Implications of the lattice oxygen participation in the liquid phase photocatalytic oxidation with nanostructured ZnO thin films on reaction products and mechanism at both 254 nm and 340 nm. *Applied Catalysis B: Environmental, 106*, 323-336. http://dx.doi.org/10.1016/j.apcatb.2011.05.033

Beauchamp, C., & Fridovich, I. (1971). Superoxide dismutase: improved assays and as assay applicable to acrylamide gels. *Analytical Biochemistry, 44*, 276-287. http://dx.doi.org/10.1016/0003-2697(71)90370-8

Bouras, P., Stathatos, E., & Lianos, P. (2007). Pure versus metal-ion-doped nanocrystalline titania for photocatalysis. *Applied Catalysis B: Environmental, 73*, 51-59. http://dx.doi.org/10.1016/j.apcatb.2006.06.007

Carp, O., Huisman, C. L., & Reller, A. (2004). Photoinduced reactivity of titanium dioxide. *Progress in Solid State Chemistry, 32*, 33-177. http://dx.doi.org/10.1016/j.progsolidstchem.2004.08.001

Chumcheng, C., Wanhong M., & Zhao, J. (2010). Semiconductor-mediated Photodegradation of pollutants under visible-light irradiation. *Chemical Society Reviews, 39*, 4206-4219. http://dx.doi.org/10.1039/b921692h

Das, C. K., & Misra, H. P. (2004). Hydroxyl radical scavenging and singlet oxygen quenching properties of polyamines. *Molecular and cellular Biochemistry, 262*, 127-133. http://dx.doi.org/10.1023/B:MCBI.0000038227.91813.79

Foote, C. S. (1991). Definition of Type-I and Type-Ii Photosensitized Oxidation. *Photochemistry and Photobiology, 54*, 659-659. http://dx.doi.org/10.1111/j.1751-1097.1991.tb02071.x

Friedmann, D., Mendive, C., & Bahnemann, D. (2010). TiO_2 for water treatment: Parameters affecting the kinetics and mechanisms of photocatalysis. *Applied Catalysis B: Environmental, 99*, 398-406. http://dx.doi.org/10.1016/j.apcatb.2010.05.014

Fu, Y., Chen, H., Sun, X., & Wang, X. (2012). Combination of cobalt ferrite and graphene: High-performance and recyclable visible-light photocatalysis. *Applied Catalysis B: Environmental, 111-112*, 280–287. http://dx.doi.org/10.1016/j.apcatb.2011.10.009

Goldstein, S., & Czapski, G. (1984). Mannitol as an OH Scavenger in Aqueous-Solutions and in Biological-Systems. *International Journal of Radiation Biology, 46*, 725-729. http://dx.doi.org/10.1080/09553008414551961

Guo, J., Li, J., Yin, A., Fan, K., & Dai, W. (2010). Photodegradation of Rhodamine B on Sulfur Doped ZnO/TiO_2 Nanocomposite Photocatalyst under Visible-light Irradiation. *Chinese Journal of Chemistry, 28*, 2144-2150.

http://dx.doi.org/10.1002/cjoc.201090355

Guo, M. Y., Ng, A. M. C., Liu, F., Djuri A. B. & Chan, W. K. (2011). Photocatalytic activity of metal oxides. The role of holes and OH radicals. *Applied Catalysis B: Environmental, 107*, 150-157. http://dx.doi.org/10.1016/j.apcatb.2011.07.008

He, Z., Sun, C., Yang, S., Ding, Y., He, H., & Wang, Z. (2009). Photocatalytic degradation of Rhodamine B by Bi_2WO_6 with electron accepting agent under microwave irradiation: Mechanism and pathway. *Journal of Hazardous Materials, 162*, 1477-1486.

He, Z., Yang, S., Ju, Y., & Sun, C. (2009b). Microwave photocatalytic degradation of Rhodamine B using TiO_2 supported on activated carbon: Mechanism implication. *Journal of Environmental Sciences, 21*, 268-272. http://dx.doi.org/10.1016/j.jhazmat.2008.06.047

Hirakawa, K, Mori, M., Yoshida, M., Oikawa, S., & Kawanishi, S. (2004). Photo-irradiated titanium dioxide catalyzes site specific DNA damage via generation of hydrogen peroxide. *Free Radical Research, 38*, 439-447. http://dx.doi.org/10.1080/1071576042000206487

Im, J. S., Yun, S.-M., & Lee, Y.-S. (2009). Investigation of multielemental catalysts based on decreasing the band gap of titania for enhanced visible light photocatalysis. *Journal of Colloid and Interface Science, 336*, 183-188. http://dx.doi.org/10.1016/j.jcis.2009.03.078

Joshi, P. C. (1985). Comparison of the DNA-Damaging Property of Photosensitized Riboflavin Via Singlet Oxygen ($^1O_2$) and Superoxide Radical ($O_2^{-}\cdot$) Mechanisms. *Toxicology Letters, 26*, 211-217. http://dx.doi.org/10.1016/0378-4274(85)90169-9

Joshi, P. C. (1998). Copper (II) as an efficient scavenger of singlet molecular oxygen. *Indian Journal of Biochemistry & Biophysics, 35*(4), 208-215.

Kment, S., Kmentova, H., Kluson, P., Krysa, J., Hubicka, Z., Cirkva, V., … Jastrabik, L. (2010). Notes on the photo-induced characteristics of transition metal-doped and undoped titanium dioxide thin films. *Journal of Colloid and Interface Science, 348*, 198-205. http://dx.doi.org/10.1016/j.jcis.2010.04.002

Kozuka, H., Zhao, G., & Yoko, T. (1996). Sol-gel preparation and photoelectrochemical properties of TiO_2 films containing Au and Ag metal particles. *Thin Solid Films, 277*, 147-154. http://dx.doi.org/10.1016/0040-6090(95)08006-6

Krajilc, I., & El Mohsni, S. (1978). A new method for the detection of singlet oxygen in aqueous solution. *Photochemistry and Photobiology, 28*, 577-581. http://dx.doi.org/10.1111/j.1751-1097.1978.tb06972.x

Kwon, C. H., Shin, H., Kim, J. H., Choi, W. S., & Yoon, K. H. (2004). Degradation of methylene blue via photocatalysis of titanium dioxide. *Materials Chemistry and Physics, 86*, 78-82. http://dx.doi.org/10.1016/j.matchemphys.2004.02.024

Lamberts, J. J. M., & Neckers, D. C. (1985). Rose-Bengal Derivatives as Singlet Oxygen Sensitizers. *Tetrahedron, 41*, 2183-2190.

Libanori, R., Giraldi, T. R., Longo, E., Leite, E. R., & Ribeiro, C. (2009). Effect of TiO_2 surface modification in Rhodamine B photodegradation. *Journal of SOL-GEL Science and Technology, 49*, 95-100. http://dx.doi.org/10.1007/s10971-008-1821-1

Liu, R., Ye, H., Xiong, X., & Liu, H. (2009). Fabrication of TiO_2/ZnO composite nanofibers by electrospinning and their photocatalytic property. *Materials Chemistry and Physics, 121*, 432-439. http://dx.doi.org/10.1016/j.matchemphys.2010.02.002

MacCormack, M. A. (2008). Photodynamic therapy in dermatology: An update on applications and outcomes. *Seminars in Cutaneous Medicine and Surgery, 27*, 52-62. http://dx.doi.org/10.1016/j.sder.2007.12.001

Macyk, W., & Kisch, H. (2001). Photosensitization of crystalline and amorphous titanium dioxide by platinum(IV) chloride surface complexes. *Chemistry-a European Journal, 7*, 1862-1867. http://dx.doi.org/10.1002/1521-3765(20010504)7:9<1862::AID-CHEM1862>3.0.CO;2-G

Mills, A., & Le Hunte, S. (1997). An overview of semiconductor photocatalysis. *Journal of Photochemistry and Photobiology A: Chemistry, 108*, 1-35. http://dx.doi.org/10.1016/S1010-6030(97)00118-4

Obuya, E. A., Harrigan, W., Andala, D. M., Lippens, J., Keane, T. C., & Jones Jr, W. E. (2011). Photodeposited Pd nanoparticle catalysts supported on photoactivated TiO_2 nanofibers. *Journal of Molecular Catalysis A: Chemical, 340*, 89-98. http://dx.doi.org/10.1016/j.molcata.2011.03.016

Pasale, J. A., Mims, L. C., Greenberg, M. H., D. S., G., & Chronister, E. (1976). Riboflavin and bilirubin response during phototherapy. *Pediatric Research, 10*, 854-856. http://dx.doi.org/10.1203/00006450-197610000-00008

Pathak, M. A., & Joshi, P. C. (1983). The Nature and Molecular-Basis of Cutaneous Photosensitivity Reactions to Psoralens and Coal-Tar. *Journal of Investigative Dermatology, 80*, S66-S74. http://dx.doi.org/10.1038/jid.1983.18

Pillay, A. E., & Salih, F. M. (2004). Gamma radiolysis and solar photolysis of bilirubin: similarities and differences. *Journal of Radiolytical and Nuclear Chemistry, 261*, 211-214. http://dx.doi.org/10.1023/B:JRNC.0000030959.94570.d5

Sakthivel, S., Hidalgo, M. C, Bahnemann, D. W., Geissen, S. U., Murugesan, V., & Vogelpohl, A. (2006). A fine route to tune the photocatalytic activity of TiO_2. *Applied Catalysis B: Environmental, 63*, 31-40. http://dx.doi.org/10.1016/j.apcatb.2005.08.011

Seaver, L. C. & Imlay, J. A. (2001). Alkyl hydroperoxide reductase is the primary scavenger of endogenous hydrogen peroxide in Escherichia coli. *Journal of Bacteriology, 183*, 7173-7181. http://dx.doi.org/10.1128/JB.183.24.7173-7181.2001

Seery, M. K. George, R. Floris, P., & Pillai, S. C. (2007). Silver doped titanium dioxide nanomaterials for enhanced visible light photocatalysis. *Journal of Photochemistry and Photobiology A: Chemistry, 189*, 258-263. http://dx.doi.org/10.1016/j.jphotochem.2007.02.010

Smith., K. C. (Ed.). (1989). *The Science of Photobiology*. New York.

Wang, H.-W., Lin, H.-C., Kuo, C.-H., Cheng, Y.-L., & Yeh, Y.-C. (2008). Synthesis and photocatalysis of mesoporous anatase TiO_2 powders incorporated Ag nanoparticles. *Journal of Physics and Chemistry of Solids, 69*, 633-636. http://dx.doi.org/10.1016/j.jpcs.2007.07.052

Wang, J., Uma, S., & Klabunde, K. J. (2004). Visible light photocatalysis in transition metal incorporated titania-silica aerogels. *Applied Catalysis B: Environmental, 48*, 151-154. http://dx.doi.org/10.1016/j.apcatb.2003.10.006

Wang, Z., Chen, C., Wu, F., Zou, B., Zhao, M., Wang, J., & Feng, C. (2009). Photodegradation of rhodamine B under visible light by bimetal codoped TiO_2 nanocrystals. *Journal of Hazardous Materials, 164*, 615-620. http://dx.doi.org/10.1016/j.jhazmat.2008.08.041

Wu, T., Liu, G., & Zhao, J. (1998). Photoassisted Degradation of Dye Pollutants. V. Self-Photosensitized Oxidative Transformation of Rhodamine B under Visible Light Irradiation in Aqueous TiO_2 Dispersions. *Journal of Physical Chemistry B, 102*, 5845-5851. http://dx.doi.org/10.1021/jp980922c

Yalda, Y., Murat, K., & Zekiye, C. (2010). Fe^{+3}-doped TiO_2: A combined experimental and computational approach to the evaluation of visible light activity. *Applied Catalysis B: Environmental, 99*(3-4), 469-477. http://dx.doi.org/10.1016/j.apcatb.2010.05.013

Yu, K., Yang, S. G., He, H., Sun, C., Gu, C. G., & Ju, Y. M. (2009). Visible Light-Driven Photocatalytic Degradation of Rhodamine B over $NaBiO_3$: Pathways and Mechanism. *Journal of Physical Chemistry A, 113*, 10024-10032. http://dx.doi.org/10.1021/jp905173e

Zhang, L. Z., Ai, Z. H., Xiao, H. Y., Mei, T., Liu, J., Deng, K. J., & Qiu, J. R. (2008). Electro-fenton degradation of Rhodamine B based on a composite cathode of Cu_2O nanocubes and carbon nanotubes. *Journal of Physical Chemistry C, 112*, 11929-11935. http://dx.doi.org/10.1021/jp803243t

Zhu, B. L., Li, K. R., Zhou, J., Wang, S. R., Zhang, S. M., Wu, S. H., & Huang, W. P. (2008). The preparation of palladium-modified TiO_2 nanofibers and their photocatalytic performance. *Catalysis Communications, 9*, 2323-2326. http://dx.doi.org/10.1016/j.catcom.2008.05.019